Materials Science for Energy Technologies 2 (2019) 329–336

Contents lists available at ScienceDirect

Materials Science for Energy Technologies

journal homepage: www.keaipublishing.com/en/journals/materials-science-for-energy-technologies

Synthesis, characterization and application of CdS/ZnO nanorod heterostructure for the photodegradation of Rhodamine B dye

Kayode Adesina Adegoke [a,b,*], Muzaffar Iqbal [c], Hitler Louis [d], Olugbenga Solomon Bello [b,*]

[a] Department of Chemistry, University of Pretoria, Pretoria 0002, South Africa
[b] Department of Pure and Applied Chemistry, Ladoke Akintola University of Technology, P.M.B. 4000 Ogbomoso, Oyo State, Nigeria
[c] Department of Chemistry, Quaid-I-Azam University, Islamabad 45320, Pakistan
[d] Department of Pure and Applied Chemistry, University of Calabar, P. M. B 1115 Calabar, Cross River State, Nigeria

ARTICLE INFO

Article history:
Received 10 December 2018
Revised 23 February 2019
Accepted 26 February 2019
Available online 23 March 2019

Keywords:
Photocatalyst
Nanorod
Photodegradation
Rhodamine B
Hydrothermal

ABSTRACT

CdS/ZnO photocatalyst were prepared by two steps via hydrothermal and photochemical method for the photodegradation of Rhodamine B (RhB) dye. The structural and morphological features of both pure ZnO nanorod and CdS/ZnO heterostructures were carefully characterized using various techniques including UV/Vis spectroscopy, XRD, SEM, EDX and EIS. The UV/Vis absorption spectra revealed that absorption performance of heterostructure is extended toward the visible light regions. Photocatalytic activity of both ZnO nanorod and CdS/ZnO heterostructures were investigated for the photodegradation of RhB dye. It was found that CdS/ZnO heterostructure prepared with 30 min light illumination shows the best photocatalytic efficiency than the one at 15 min and pure ZnO nanorod. The better and enhanced photocatalytic efficiency of CdS/ZnO heterostructure was ascribed to the high charge separation efficiency. The maximum photocatalytic efficiency of 85% was achieved within 8 h with the CdS/ZnO-30 min photocatalyst. This work revealed that composite such as CdS/ZnO heterostructure has better photocatalytic efficiency that pure ZnO nanorod.

1. Introduction

Photocatalysis is an auspicious technique for the reduction of organic pollutants both in water and air. Due to their numerous important applications, semiconductor nanostructures have been of valuable attention in combating problems associated with the use of organic pollutants such as dyes. Among numerous metal-oxide semiconductors, TiO_2 and ZnO were used broadly as photocatalysts owing to their extraordinary photocatalytic activity, appropriate band gap and stability against photocorrosion [1–4]. Zinc oxide (ZnO) has a wide band gap semiconductor that is gaining widespread attention in photocatalytic applications because of its higher exciton binding energy of 60 meV [1,2,5–18], high electron mobility, break-down strength, its low cost, extraction stability and non-toxic nature [2,4,11–16]. Owing to the wide band gap, high electron and hole recombination and lower faradic efficiency, the practical application of the ZnO is limited [2,19–22]. In order to address this problem, the ZnO is coupled with another semiconductors with narrow band gap thereby enhancing the absorption range and as a result increase photocatalytic efficiency [5,9,18,23,24]. In the literature, a number of narrow band gap semiconductors have been reported which are combined with ZnO in order to increase the photocatalytic efficiency. Example of such semiconductors are TiO_2–ZnO [25–27], Au-ZnO [13,15,28,29], NiO/ZnO [30] ZnO–WO_3 [31,32], ZnO–Fe_2O_3 [31,32], ZnO/V_3O_4 [8], $Zn_xCd_{1-x}S$ [22], ZnO/Clay [10], In_2O_3/ZnO [33], ZnO-ZnS [17,34,35], Ag-N-ZnO [16], ZnO–Ag_2S [36], RuO_2-ZnO [37], $CuInS_2$/ZnO [38], CuO-ZnO [39,40], Mn_2O_3-ZnO [41], Ag_3PO_4–ZnO [42], V_2O_5–ZnO [13], ZnO–CdO[43] MoO_3–ZnO [28], Nb_2O_5–ZnO [44], Cellulose–PVC–ZnO [45] and Fe_3O_4@ZnO [46].

* Corresponding authors at: Department of Chemistry, University of Pretoria, Pretoria 0002, South Africa (K.A. Adegoke). Department of Pure and Applied Chemistry, Ladoke Akintola University of Technology, P.M.B. 4000 Ogbomoso, Oyo State, Nigeria. (O.S Bello)
E-mail addresses: kwharyourday@gmail.com (K.A. Adegoke), osbello@lautech.edu.ng (O.S. Bello).
Peer review under responsibility of KeAi Communications Co., Ltd.

Production and hosting by Elsevier

https://doi.org/10.1016/j.mset.2019.02.008
2589-2991/

On the other hand, CdS remains one of the familiar semiconductors having narrow direct band gap (2.4 eV) and widely employed as a visible light photocatalyst [47,48]. It is also used as a photosensitizer in many photochemical cells of numerous wide band gap semiconductor photoanodes [49–51]. Combining ZnO and CdS to form heterostructure have numerous importance because the subsequent product has the ability of improving their physical and chemical properties. The band energy structures of ZnO and CdS are suitable to stimulate the transfer of electron processes where photogenerated electron can drift from CdS to ZnO [22,43,47,49,50,52] and the charge transporters become physically detached upon generations.

In this work, we prepared CdS/ZnO heterostructures by simple reproducible photodeposition technique. The contents of CdS were varied by adjusting the time of irradiation. The CdS/ZnO and ZnO heterostructures were characterized using different techniques. The CdS/ZnO heterostructures was used as a photocatalyst in the photocatalytic degradation of Rhodamine B (RhB) dye.

2. Materials and methods

2.1. Reagents used

All chemicals: Zinc Acetate dihydrate ($Zn(OAc)_2{\cdot}2H_2O$), Hexamethylenetetramine (HMT) Cadmium Nitrate Tetrahydrate ($Cd(NO_3)_2{\cdot}4H_2O$) and Sulphur were obtained from Merck and Sigma Aldrich. These chemicals are used without further purification.

2.2. Synthesis of ZnO nanorod and CdS/ZnO heterostructure.

Area controlled (Fluorine-doped Tin Oxide) FTO glass (1 cm × 2 cm) was cleaned by ultrasonic processing in sequence of washing with water, detergent/water mixture, MilliQ-water, ethanol, acetone and isopropanol. The FTO substrate was dried using nitrogen gas and then transferred into an oven for 2 h at 60 °C. The FTO substrate was further cleaned by ultrasonic processing in ethanol followed by MilliQ-water rinsing and dried by nitrogen gas. The ZnO film was grown on FTO substrate by first preparing a thin ZnO seed-layer. The FTO substrate was transferred to Lesker Lab 18 and heated to 200 °C with background pressure of 2.0×10^{-7} Torr. The ZnO seed layer was sputtered at 120 W from zinc (99.99%, Grikin) by reacting with 50 standard cubic centimeter per minute (sccm) Ar and 14.4 sccm O_2.

The ZnO nanorod array was fabricated on FTO glass by hydrothermal method. In the hydrothermal process, 100 mL precursor was prepared by mixing 0.22 g $Zn(OAc)_2{\cdot}2H_2O$, 0.14 g hexamethylenetetramine (HMT) and 100 mL MilliQ-water to obtain a clear solution which was transferred into 150 mL Teflon-lined stainless steel Autoclave and ZnO-film/FTO glass was fixed in the polytetrafluoroethylene (PTFE) lining face down. The lining was sealed in the Autoclave and then put in oven for 8 h at 90 °C. The temperature of the Autoclave was allowed to cool down to room temperature; then the as-synthesized ZnO-nanorod was removed and then washed with ethanol and MilliQ-water several times. It was thereafter dried for 4 h at 60 °C in an oven.

Similarly, CdS particles were successively deposited on ZnO using a photodeposition technique. 30 mg of S_8 and 450 mg of $Cd(NO_3)_2{\cdot}4H_2O$ were added in a solution mixture of water (20 mL) and ethanol (30 mL). Nitrogen gas was then bubbled into the suspension for 30 min in the dark to remove other dissolved gasses. The ZnO films were placed in the solution, then the light was illuminated using the 300 W Xenon lamp at room temperature at various time intervals (15 and 30 min respectively). Then the final products were washed several times with MilliQ-water and ethanol and the sample was allowed to dry in a vacuum overnight.

2.3. Determination of photocatalytic activities of ZnO nanorod and CdS/ZnO heterostructure.

The solution of RhB dye was prepared by dissolving 1 μmol of RhB dye in 20 mL ethanol. The as-synthesized ZnO and CdS/ZnO nanoparticle samples were then used to measure the photodegradation of RhB dye in aqueous solution. The efficiency of ZnO and CdS/ZnO nanoparticles were investigated under UV/Vis light. To study photocatalytic activity of ZnO nanorod and CdS/ZnO heterostructure samples, 2 mL of colloidal solution and 2 mL of ethanol were mixed thoroughly with 200 μL RhB dye solution separately in plastic cuvettes. ZnO nanorod film and CdS/ZnO heterostructure were placed in the reactor containing dye solution. Light was illuminated from the 300 W Xe lamps on the solution. An aliquot of the suspension was taken at different time intervals from the reactor. The UV/Vis spectrophotometer was used for measuring the absorbance of the solutions at 553 nm wavelength to account for the effects of irradiation time as a function of the RhB dye concentrations.

2.4. Characterization of ZnO and CdS/ZnO nanorods

Optical absorption spectra of both ZnO nanorod, CdS/ZnO nanorod and the RhB solutions were recorded in the range of 300–800 nm on a Perkin-Elmer Lambda 25 UV/Vis–NIR spectrometer. The X-ray diffraction (XRD) of ZnO nanorod and CdS/ZnO heterostructures were taken using a Rigaku SmartLab diffractometer at room temperature. The CuK-α radiation (λ = 1.5418 Å) was generated at 45 kV and 200 mA. The two-dimensional diffraction patterns (2θ) were reported in a range from 20° to 80° in steps of 0.02° and a counting time of 2 sec/step. Data matching was carried out on Diffrac.Eva software (version 2.0). The surface morphology of the ZnO nanorod and CdS/ZnO heterostructure were examined using Field Emission Scanning Electron Microscope (FESEM) (JEOL JSM7401F) under the conditions of 1.5 keV and 3 mm working distance. This is a versatile imaging technique that is based on electron-material interaction, capable of producing image(s) of the surface of samples. The principle is based on bombarding the surface of the sample with the electron beam to re-emit certain particles; the electrons then interact with atoms in the sample, thus producing quantitative and qualitative information pertaining to particle morphology and surface appearance of samples. Various detectable signals containing specific information concerning the sample surface topology and compositions are analyzed by a range of detectors to give three-dimensional image(s). Energy Dispersive X-Ray (EDX, JEOL, JSM6500F, Japan) analysis was carried out on both ZnO nanorod and CdS/ZnO heterostructure samples to determine the elemental components.

2.5. Photodegradation activity experiments

The photocatalytic activity of the ZnO nanorod and CdS/ZnO nanorod samples on RhB dye were determined using photodegradation technique under activated sunlight from a 300 W Xenon lamp at normal conditions. Each of ZnO nanorod and CdS/ZnO photocatalyst was placed in 100 mL containing aqueous solution of 5.0×10^{-5} M RhB dye. Prior to irradiation studies, the electrodes were positioned in solution in the dark for 2 h to attain an adsorption/desorption equilibrium. The zero-time reading was obtained from the blank solution kept in the dark but otherwise treated similarly to the irradiated sample. After a specific time of radiation, small volume of the solutions was withdrawn for determination of RhB dye concentration. The processes of photocatalytic degradation were monitored by UV/Vis spectrophotometer. Blank experiments without addition of catalyst and with the catalyst in the dark were also carried out.

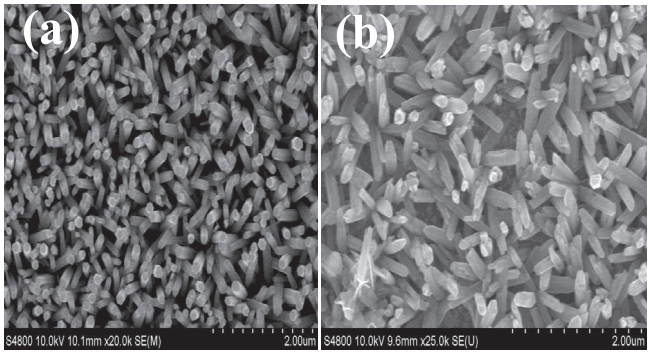

Fig. 1. FE-SEM images of (a) ZnO nanorod and (b) CdS/ZnO heterostructure.

3. Results and discussions

3.1. Formation and structural characteristics

Fig. 1 presents the SEM images of ZnO and CdS/ZnO heterostructures. It clearly shows the formation of nanorods of both ZnO and CdS/ZnO heterostructures grown on FTO substrate. The substrate was fully covered with the ZnO nanorods. It was observed that the uniform ZnO nanorods are vertically aligned into well-defined arrays and have a high surface density (Fig. 1a). However, when CdS was deposited on ZnO under illumination treatment, the growth between ZnO nanorods and CdS nanoparticle occurred immediately. As shown in Fig. 1b, uniform CdS nanoparticle was deposited on the surface of ZnO nanorods both after 15 min and 30 min illumination respectively. In addition, the growing of numerous nanoparticles having different sizes in nanometers were observed on the surface of the CdS/ZnO nanorods owing to the formation of grainy and rough structures on the CdS/ZnO surfaces; compared with those of ZnO nanorods. These were the results of molecular disorders and lattice strains, thereby resulting into difference in their ionic radii. These imply that nanoparticles were produced from the rapid reactions between the S^{2-} anions and Cd^{2+} ions occurring in the second preparatory step. This therefore resulted into the attachment on the ZnO nanorod surfaces. Importantly, these coarse and rough surface structures enhance absorption of RhB dye and reduce the incident light reflection, thereby improving photocatalytic performance greatly [52–58].

To corroborate the chemical analysis of pure ZnO nanorod and CdS/ZnO heterostructure, chemical analysis using the Energy dispersive X-ray (EDX) technique was used. It comprises of protons detection using Si–Li solid detector called detection by energy dispersions. The photon energy, X, is characteristic of the atom. The peaks (lines spectra) obtained corresponds to individual photon X of a given energy and each corresponding to a particular element [59]. The intensities of the characteristic lines are proportional to the concentrations of the elements; these analyses are quantitative in nature (Fig. 2). Nevertheless, there are factors of corrections which are dependent on the sample compositions and the experimental parameters (such as the incidental beam energy and angle). As a result on this, only semi-quantitative analyzes are considered in this study. The limit of detection was positioned at the 0.1–1% concentrations for elements with average or light atomic weights, with the exception of superposition of characteristic peaks which are unfavorable (see the inset in Fig. 2). Fig. 2 shows the EDX spectra of pure ZnO and CdS/ZnO. In ZnO sample, only Zn and O elements were found, contributing to total atomic percentages of 42.66 and 57.34% respectively. Whereas in CdS/ZnO, there were existences of Zn, O, Cd and S elements having atomic percentages of 47.48, 51.44, 0.47 and 0.61% respectively. This show that CdS successfully formed heterostructure with ZnO nanorod. The small percentage of Cd and S were as a result of a very small amount of CdS loading on the ZnO nanorod. Comparing the two samples, the increase and decrease in atomic percentages of both Zn and O observed in CdS/ZnO is an indication that CdS/ZnO would be a good and efficient photocatalyst for RhB dye degradation. EDX analysis revealed that there were no impurities in the samples.

3.2. Growth mechanism

CdS was photodeposited on the ZnO surface leading to the formation of Cd^{2+} ions reduced to Cd^0, this follows by the successive reactions with S_8 [14,23,51,60,61]. For equilibrium, the ions of Cd^{2+} were adsorbed onto the surface of ZnO in the dark condition. Upon light irradiation, ZnO got excited leading to initiation of inter-band transitions for the generation of electron-hole pair (Mechanism 1) with ethanol acting as holes-scavenger. This makes the valence band (VB) holes to escape the recombination and thereby oxidizing ethanol to $\cdot C_2H_4OH$ radical (Mechanism 2). This injects other electrons to the ZnO conduction band (CB) to form CH_3CHO and H^+ (Mechanism 3) which have stronger reducing radical ($\cdot C_2H_4OH$) [13,42,61,62]. Therefore, this resulted into the accumulation of electrons in the ZnO CB, thereby reducing the ions of Cd^{2+} to Cd^0 (Mechanism 4). The reactions between the Cd^0 and S_8 produced CdS (Mechanism 5).

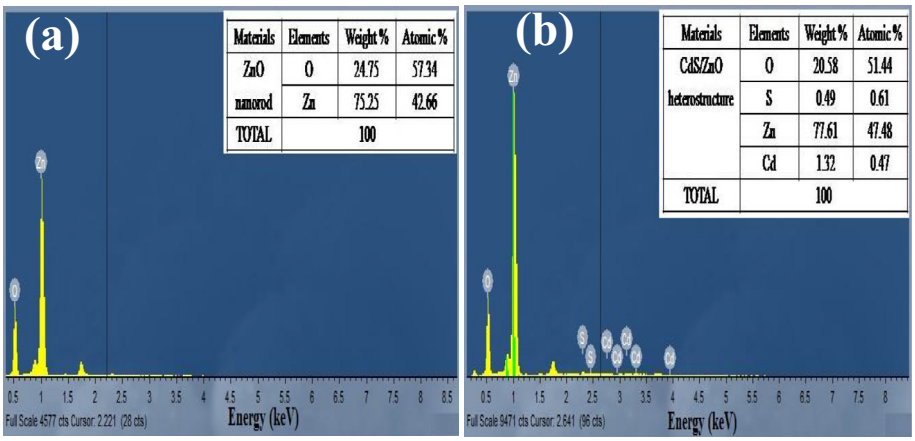

Fig. 2. (a) EDX spectrum of ZnO nanorods; (b) EDX spectrum of CdS/ZnO heterostrcutures.

Inter-band transition for the generation of electron–hole pair (Mechanism 1)

$$ZnO + h\upsilon \rightarrow ZnO(e^{-}_{CB} + h_{VB}) \quad \text{(Mechanism1)}$$

Oxidation of ethanol to $\cdot C_2H_4OH$ radical (Mechanism 2).

$$C_2H_5OH + h\upsilon^{+}_{VB} \rightarrow \cdot C_2H_4OH + H^{+} \quad \text{(Mechanism2)}$$

Injection of electrons to the ZnO conduction band (CB) to form CH_3CHO and H^+ (Mechanism 3).

$$\cdot C_2H_4OH \rightarrow \cdot CH_3CHO + H^{+} + e^{-}_{CB} \quad \text{(Mechanism3)}$$

Accumulation of electrons in the ZnO CB, reducing the ions of Cd^{2+} to Cd^0 (Mechanism 4).

$$Cd^{2+} + 2e^{-}_{CB} \rightarrow Cd^{0} \quad \text{(Mechanism4)}$$

Reaction between Cd^0 and S_8 to generate CdS (Mechanism 5).

$$8Cd^{0} + S_8 \rightarrow 8CdS \quad \text{(Mechanism5)}$$

Moreover, the XRD patterns of ZnO nanorod and CdS/ZnO heterostructure are presented in Fig. 3 with ZnO showing the formation of hexagonal wurtzite characteristic diffraction peaks (JCPDS No. 36–1451). The diffraction peaks observed were $2\theta = 26.64°$, 34.62°, 43.92°, 47.69°, 51.73°, 61.74°, 62.92°, 65.73° and 72.73° respectively. Beside the ZnO characteristic peak, one additional peak also appeared in the spectrum at $2\theta = 43.92°$ indexed to (1 1 0) which corresponds to CdS, thus confirming the successful formation of CdS/ZnO heterostructure. The peak intensity of CdS is smaller because of the small CdS-loading on the superface of ZnO nanorod. It should be noted that ZnO nanorod diffraction peaks observed in CdS/ZnO heterostructure are sharper while that of CdS which are noticeably weaker, implying that ZnO nanorod sample has a high crystalline characters while they are only smaller in the CdS sample. This observation agreed with literature [22,54,61,63,64]. No impurity peak was observed in the XRD patterns.

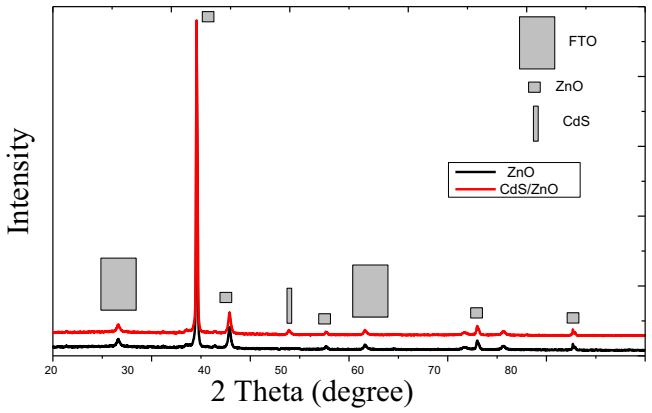

Fig. 3. XRD patterns of the ZnO nanorods and CdS/ZnO heterostructure.

3.3. Optical study

The UV/Vis-spectroscopy of pure ZnO nanorods and CdS/ZnO heterostructures were recorded from 300 to 800 nm range (Fig. 4a) in accordance with the previous works [58,65,66]. ZnO gives absorption peak at UV region (Fig. 4a). After the deposition of CdS on ZnO, the absorption peak shifted toward the visible region (Fig. 4a). Nevertheless, the UV/Vis absorption spectrum of CdS/ZnO heterostructure (Fig. 4b) show noticeable shifts in absorption peaks belonging to CdS and ZnO characteristic absorption edges confirming that these materials only comprised of CdS and ZnO. The absorption intensity of CdS/ZnO revealed higher peak than the one observed in ZnO as shown in the Fig. 4a. This signifies the impact of lesser amount of CdS on the composites during the immobilization of CdS onto ZnO.

However, the respective band gap energies of both ZnO nanorod and CdS/ZnO heterostructure were calculated using Tauc equation (Eq. (1)).

$$(\alpha h\upsilon)^{1/r} = B(h\upsilon - Eg) \quad (1)$$

where "Eg" is the band gap energy, B is a constant, υ is the frequency of the incident radiation, h is Planck's constant, α is the absorption coefficient, r is determined by the type of optical transition of a semiconductor. The band gap can be obtained by extrapolating the linear section of the plot of $(\alpha h\upsilon)^2$ vs $h\upsilon$ in the high absorption range and finding the intercept on the x-axis" [52]. For ZnO, the band gap energy was 3.14 eV (Fig. 4b) which corresponds to the literature value [58,61,67]. The band gap of CdS/ZnO is red shifted to 3.04 eV as shown in Fig. 4b. The shifting towards the visible region could be attributed to the effects of the quantum confinement on the CdS/ZnO semiconductor, which also implies that CdS/ZnO has a suitable band gap required for activation by the visible light for photodegradation of RhB dye. This observation is in agreement with previous works [58,61,67–69].

In order to find out the interfacial properties of these materials, Electrochemical Impedance Spectroscopy (EIS) which is an effective technique was used to achieve this. The EIS results are shown in the Nyquist plots (Fig. 5) of ZnO, CdS/ZnO (15 and 30 min photocatalysts). The 0.5 mM (1:1) $[Fe(CN)6]^{3-/4-}$ was used for redox

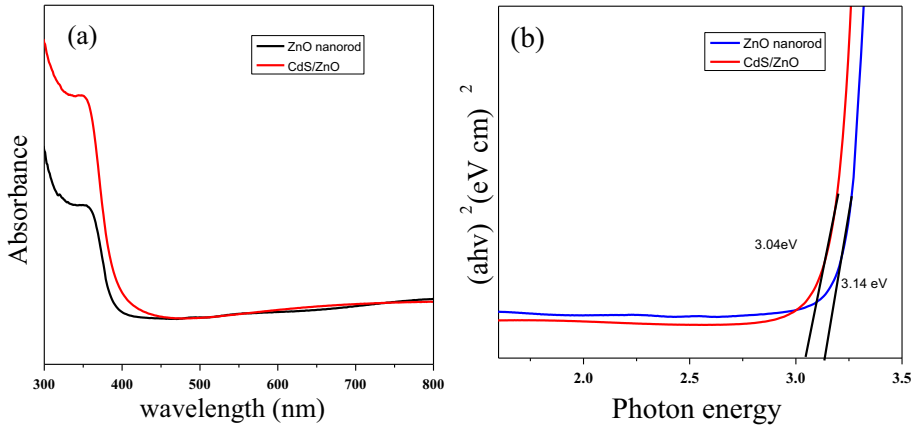

Fig. 4. UV/vis spectrum of pure ZnO nanorods and CdS/ZnO (b) Band gap estimation of pure ZnO nanorods and CdS/ZnO heterostructures.

probing. It is evidenced from the Nyquist plots that electrodes exhibited typical semicircles at higher frequency region while linear trend was detected in the lower frequency region. For the higher frequency region, the intercept was as a result of solution resistance. The diameters of semicircles in the Nyquist plot were the extents of the charge transfer resistances (Rct), which in reality controlled the kinetics of the electron transfers of the redox probe on the surfaces of the electrode. The Rct is a sensitive and direct parameter for depicting the electrodes/electrolytes interfacial properties [58,70,71]. It can be observed in Fig. 5 that ZnO electrodes demonstrated poor and inferior charge transfer kinetics in comparison with CdS/ZnO heterostructures. While 30 min CdS/ZnO exhibited the least Rct among the catalysts under study. The EIS result also confirmed the efficient charge transfer in 30 min CdS/ZnO as compared to 15 min CdS/ZnO and pure ZnO.

3.4. Determination of photocatalytic activities of ZnO nanorod and CdS/ZnO heterostructure

The photocatalytic activities of the pure ZnO nanorod and CdS/ZnO heterostructure were investigated using RhB dye as pollutant water under UV/Vis light (Fig. 6). The photocatalytic behavior of ZnO nanorod and CdS/ZnO heterostructures for different times at 25 °C under UV/Vis light irradiations are presented in Fig. 6. The photocatalytic efficiency is calculated using the equation:

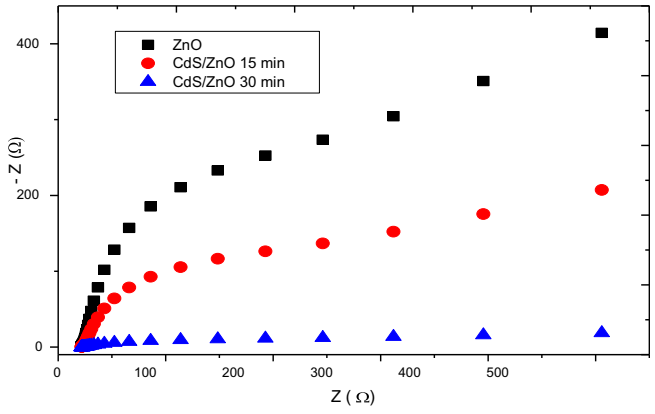

Fig. 5. Nyquist plots of the catalysts in (1:1) 0.5 mM $[Fe(CN)6]^{3-/4-}$ in the frequency range of 10 Hz–100 kHz at open circuit voltage.

$$\%\ \text{Degradation} = \frac{C_o - C_t}{C_o} \times 100 \quad (2)$$

where C_0 and C_t are the initial and final concentrations of RhB dye.

The control experiment (pure RhB dye) was firstly set up without any catalyst under visible light irradiation and the result gave no degradation efficiency (Fig. 6a). This study reveals that RhB dye was not self-degraded under visible light irradiation system when catalyst was not involved, thereby revealing a stable behavioral pattern and nature of RhB dye. However, for ZnO nanorod photocatalyst, the RhB dye degradation efficiency was 58%, this is lower when compared with CdS/ZnO heterostructure at 15 min with efficiency of 73% (Table 1). Whereas, for the photodegradation of RhB dye at 30 min of the light irradiation using thae same catalyst, CdS/ZnO heterostructure, the photodegradation of RhB dye gave a higher efficiency of 85% and the degradation process was completed in 30 min (Table 1). This shows that CdS/ZnO heterostructure at 30 min displayed superior photocatalytic activity than the ZnO nanorod and CdS/ZnO at 15 min light irradiation time (Fig. 6b). This indicates that introduction of CdS onto ZnO nanorod enhanced the photodegradation of RhB dye from 58% to 85% efficiency, thus proofing the excellent photocatalytic efficiency of CdS/ZnO to degrade RhB dye [58,66]. This is because in CdS/ZnO heterostructure, the photo response ranges were prolonged and light energy was absorbed under simulated sunlight irradiations. Notably, the improved photocatalytic efficiency of CdS/ZnO was characteristically an effect of inhibition of the electron–hole pair recombination by the charge transfer processes in CdS/ZnO heterostructure.

However, the kinetics of RhB dye degradation was also investigated and quantitatively compared with the photocatalytic performances of the samples, this fitted well to pseudo first-order equation:

$$kt = \ln\frac{C_o}{C_t} \quad (3)$$

Table 1
Photocatalytic efficiency and rate constant of pure ZnO and CdS/ZnO.

Samples	Photocatalytic efficiency %	Rate constant k (min)
Pure ZnO	58	0.0019
CdS/ZnO (15 min)	73	0.0036
CdS/ZnO (15 min)	85	0.0040

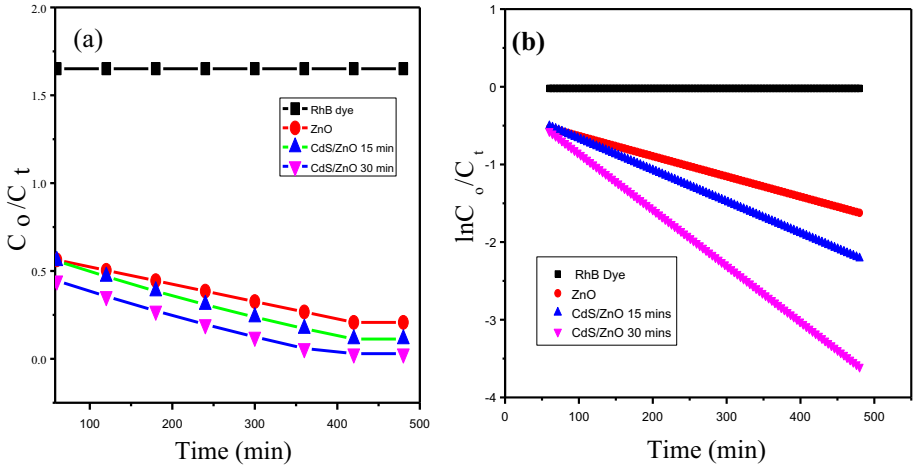

Fig. 6. Photocatalytic decomposition of RhB over different photocatalyst such as, ZnO nanorod and CdS/ZnO at different time under visible light irradiation. Reaction conditions: $C_0 = 1.03 \times 10^{-3}$ M; Catalyst loading: 0.01 g/L; (b). Determination of the apparent rate constants for RhB degradation reaction over the prepared ZnO nanorod and CdS/ZnO at different time.

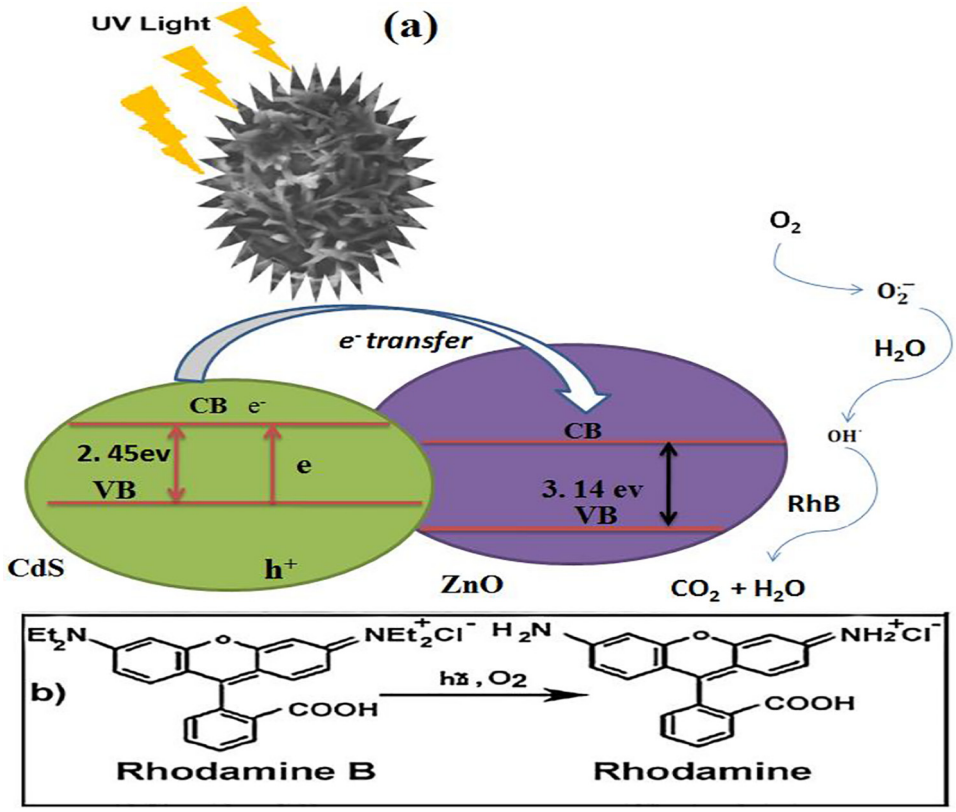

Fig. 7. The schematic (a) photodegradation process in the CdS/ZnO/RhB aqueous solution, and (b) N-deethylation of Rhodamine B to Rhodamine.

where k_t signifies the pseudo first-order rate constant (in min^{-1}) of initial degradation, C_t and C_0 are final and initial concentrations of RhB dye respectively. The rate constant, k_t, which is the slope of the linear plot of ln (C_0/C_t) against irradiation time (t) (Fig. 6b) obtained were 0.0019, 0.0036 and 0.0040 min^{-1} were observed for ZnO nanorod, CdS/ZnO (15 min) and CdS/ZnO (30 min) respectively. This implies that CdS/ZnO (30 min) exhibited higher rate constant k_t, which is more than two-fold increase than the "k_t" value observed in ZnO nanorod. This means that the amalgamation of CdS with ZnO nanorod gave an enhanced RhB dye degradation over a standard period of time.

The phenomena for CdS/ZnO having higher activities on the photocatalytic activities could be explained further by the mechanism of the reactions (see the scheme in Fig. 7). The Fig. 7 elucidates the photocatalytic reaction mechanisms, which comprise of the generation of electron–hole pairs by the incident photon, charge separation/transportation and lastly the reactions involving the oxidation/reduction of the species absorbed. Since CdS/ZnO systems have "staggered type-II" band gap alignments [72,73], it then follows that the location of CB-edge of ZnO is amidst the CB and VB of CdS (see the scheme in Fig. 7). The transfer of photoelectrons to CB facilitates the electron hole charge separation before recombination; this was as a result of the generation of electron hole pairs by the visible light. Consequently, leading to excitation in the band gap configuration of CdS. This band alignment is a major significant factor that must be taken into consideration when looking for a way to augment photocatalytic efficiencies. Fig. 7(a) shows modified diagram for band gap energy, obtainable for the synthesized photocatalyst. The position of CdS/ZnO band systems obviously elucidated the feasibilities of charge transfers from CdS to ZnO owing to CB and VB-edges of CdS having more negative charges than those of ZnO [74–76]. In order to enhance the photoresponse, a faster charge transport rate is required, which can be facilitated by the effective and close contact of the hybrid materials Fig. 7(b). The higher photodegradation efficiency of CdS/ZnO samples in comparison with ZnO nanorod could be attributed to prominent UV/Vis light absorption, high charge separation carrier and a succeeding carrier diffusion on the CdS/ZnO surface [67,77]. This implies that composite structural arrangements decreased the charge recombination electron-hole pair on the surface of CdS/ZnO heterostructure. On the other hand, the lower efficiency observed in ZnO implies that the ZnO surfaces are protected from incident light leading to more scattering effects of UV/Vis light penetration, thereby, inhibiting the light absorption by the ZnO nanorod. Therefore, CdS/ZnO heterostructures demonstrated a superior photocatalytic performance than ZnO precursor under the simulated sunlight (Table 1).

4. Conclusion

In this study, we have successfully synthesized ZnO and CdS/ZnO photocatalysts by hydrothermal method for the photodegradation of RhB dye. The characterization of the as-synthesized nanostructure samples were performed by various techniques including UV/Vis spectroscopy, XRD, SEM, EDX and EIS respectively. The photocatalysts developed in this study demonstrated high and wide surface areas, the light absorptions pattern extended to the UV/visible regions, thus their photo catalytic activities are enhanced. Both pure ZnO nanorod, CdS/ZnO heterostructures at 15 and 30 min photodeposition times were compared. It was found that 30 min CdS/ZnO photocatalyst is highly photoactive than pure ZnO nanorod and 15 min CdS/ZnO. The high photodegradation efficiency and enhanced photocatalytic activity was ascribed to an increased in charge separation efficiencies of CdS/ZnO heterostructures at 30 min.

Conflict of interest

No conflict of interest is declared by the authors.

Acknowledgements

Authors acknowledge the support obtained from The World Academy of Science (TWAS) in form of Research grants; Research Grant number: 11-249 RG/CHE/AF/AC_1_UNESCO FR: 3240262674 (2012), 15-181 RG/CHE/AF/AC_1_:3240287083 (2015), 2016 TET Fund Institution Based Research Intervention (TETFUND/DESS/UNI/OGBOMOSO/RP/VOL. IX) and NRF-TWAS for Doctoral Fellowship award given to the first author (UID: 105453 & Reference: SFH160618172220) respectively.

Appendix A. Supplementary data

Supplementary data to this article can be found online at https://doi.org/10.1016/j.mset.2019.02.008.

References

[1] E.M. Kaidashev, M. Lorenz, H. Von Wenckstern, A. Rahm, H.C. Semmelhack, K. H. Han, G. Benndorf, C. Bundesmann, H. Hochmuth, M. Grundmann, High electron mobility of epitaxial ZnO thin films on c-plane sapphire grown by multistep pulsed-laser deposition, Appl. Phys. Lett. 82 (2003) 3901–3903, https://doi.org/10.1063/1.1578694.

[2] S. Maiti, S. Pal, K.K. Chattopadhyay, Recent advances in low temperature, solution processed morphology tailored ZnO nanoarchitectures for electron emission and photocatalysis applications, Cryst. Eng. Comm. 17 (2015) 9264–9295, https://doi.org/10.1039/c5ce01130b.

[3] M. Samadi, M. Zirak, A. Naseri, E. Khorashadizade, A.Z. Moshfegh, Recent progress on doped ZnO nanostructures for visible-light photocatalysis, Thin Solid Films 605 (2016) 2–19, https://doi.org/10.1016/j.tsf.2015.12.064.

[4] M. Shaban, M. Zayed, H. Hamdy, Nanostructured ZnO thin films for self-cleaning applications, RSC Adv. 7 (2017) 617–631, https://doi.org/10.1039/c6ra24788a.

[5] J. Fowsiya, G. Madhumitha, N.A. Al-Dhabi, M.V. Arasu, Photocatalytic degradation of Congo red using Carissa edulis extract capped zinc oxide nanoparticles, J. Photochem. Photobiol. B Biol. 162 (2016) 395–401, https://doi.org/10.1016/j.jphotobiol.2016.07.011.

[6] Y.F. Zhukovskii, S. Piskunov, O. Lisovski, E. Spohr, R.A. Evarestov, Quantum chemical simulations of doped ZnO nanowires for photocatalytic hydrogen generation, Phys. Status Solidi Basic Res. 253 (2016) 2120–2128, https://doi.org/10.1002/pssb.201600452.

[7] R. Atchudan, T.N.J.I. Edison, S. Perumal, M. Shanmugam, Y.R. Lee, Direct solvothermal synthesis of zinc oxide nanoparticle decorated graphene oxide nanocomposite for efficient photodegradation of azo-dyes, J. Photochem. Photobiol. A Chem. 337 (2017) 100–111, https://doi.org/10.1016/j.jphotochem.2017.01.021.

[8] S. Harish, M. Sabarinathan, J. Archana, M. Navaneethan, S. Ponnusamy, C. Muthamizhchelvan, H. Ikeda, Y. Hayakawa, Functional properties and enhanced visible light photocatalytic performance of V_3O_4 nanostructures decorated ZnO nanorods, Appl. Surf. Sci. 418 (2017) 171–178, https://doi.org/10.1016/j.apsusc.2017.02.261.

[9] C. Vidya, C. Manjunatha, M.N. Chandraprabha, M. Rajshekar, M.A.L. Antony Raj, Hazard free green synthesis of ZnO nano-photo-catalyst using Artocarpus Heterophyllus leaf extract for the degradation of Congo red dye in water treatment applications, J. Environ. Chem. Eng. 5 (2017) 3172–3180, https://doi.org/10.1016/j.jece.2017.05.058.

[10] H. Bel Hadjltaief, S. Ben Ameur, P. Da Costa, M. Ben Zina, M. Elena Galvez, Photocatalytic decolorization of cationic and anionic dyes over ZnO nanoparticle immobilized on natural Tunisian clay, Appl. Clay Sci. 152 (2018) 148–157, https://doi.org/10.1016/j.clay.2017.11.008.

[11] Ü. Özgür, Y.I. Alivov, C. Liu, A. Teke, M.A. Reshchikov, S. Doğan, V. Avrutin, S.J. Cho, H. Morko, A comprehensive review of ZnO materials and devices, J. Appl. Phys. 98 (2005) 1–103, https://doi.org/10.1063/1.1992666.

[12] D.C. Look, Recent advances in ZnO materials and devices, Mater. Sci. Eng. B Solid-State Mater. Adv. Technol. 80 (2001) 383–387, https://doi.org/10.1016/S0921-5107(00)00604-8.

[13] H. Yin, K. Yu, C. Song, R. Huang, Z. Zhu, Synthesis of Au-decorated V2O5@ZnO heteronanostructures and enhanced plasmonic photocatalytic activity, ACS Appl. Mater. Interfaces 6 (2014) 14851–14860, https://doi.org/10.1021/am501549n.

[14] Y. Zhao, L. Liu, T. Cui, G. Tong, W. Wu, Enhanced photocatalytic properties of ZnO/reduced graphene oxide sheets (rGO) composites with controllable morphology and composition, Appl. Surf. Sci. 412 (2017) 58–68, https://doi.org/10.1016/j.apsusc.2017.03.207.

[15] S. Kuriakose, K. Sahu, S.A. Khan, A. Tripathi, D.K. Avasthi, S. Mohapatra, Facile synthesis of Au-ZnO plasmonic nanohybrids for highly efficient photocatalytic degradation of methylene blue, Opt. Mater. (Amst) 64 (2017) 47–52, https://doi.org/10.1016/j.optmat.2016.11.035.

[16] T. Welderfael, O.P. Yadav, A.M. Taddesse, J. Kaushal, Synthesis, characterization and photocatalytic activities of Ag-N-Codoped ZnO nanoparticles for degradation of methyl red, Bull. Chem. Soc. Ethiop. 27 (2013) 221–232, https://doi.org/10.4314/bcse.v27i2.7.

[17] A. Sadollahkhani, O. Nur, M. Willander, I. Kazeminezhad, V. Khranovskyy, M.O. Eriksson, R. Yakimova, P.O. Holtz, A detailed optical investigation of ZnO@ZnS core-shell nanoparticles and their photocatalytic activity at different pH values, Ceram. Int. 41 (2015) 7174–7184, https://doi.org/10.1016/j.ceramint.2015.02.040.

[18] C.B. Ong, A.W. Mohammad, R. Rohani, M.M. Ba-Abbad, N.H.H. Hairom, Solar photocatalytic degradation of hazardous Congo red using low-temperature synthesis of zinc oxide nanoparticles, Process Saf. Environ. Prot. 104 (2016) 549–557, https://doi.org/10.1016/j.psep.2016.04.006.

[19] M. Çopuroğlu, L.H.K. Koh, S. O'Brien, G.M. Crean, Comparative characterisation of zinc oxide thin films prepared from zinc acetate with or without water of hydration via the sol-gel method, J. Sol-Gel Sci. Technol. 52 (2009) 432–438, https://doi.org/10.1007/s10971-009-2016-0.

[20] S. O'Brien, M.G. Nolan, M. Çopuroglu, J.A. Hamilton, I. Povey, L. Pereira, R. Martins, E. Fortunato, M. Pemble, Zinc oxide thin films: characterization and potential applications, Thin Solid Films (2010) 4515–4519, https://doi.org/10.1016/j.tsf.2009.12.020.

[21] S.K. Arya, S. Saha, J.E. Ramirez-Vick, V. Gupta, S. Bhansali, S.P. Singh, Recent advances in ZnO nanostructures and thin films for biosensor applications: review, Anal. Chim. Acta 737 (2012) 1–21, https://doi.org/10.1016/j.aca.2012.05.048.

[22] Y. Jin, H. Zhang, C. Song, L. Wang, Q. Lu, F. Gao, Hollow ZnxCd1-xS nanospheres with enhanced photocatalytic activity under visible light, Sci. Rep. 6 (2016), https://doi.org/10.1038/srep29997.

[23] M.H. Malakooti, H.S. Hwang, H.A. Sodano, Morphology-controlled ZnO nanowire arrays for tailored hybrid composites with high damping, ACS Appl. Mater. Interfaces 7 (2015) 332–339, https://doi.org/10.1021/am506272c.

[24] A. Balcha, O.P. Yadav, T. Dey, Photocatalytic degradation of methylene blue dye by zinc oxide nanoparticles obtained from precipitation and sol-gel methods, Environ. Sci. Pollut. Res. 23 (2016) 25485–25493, https://doi.org/10.1007/s11356-016-7750-6.

[25] E.S. Araújo, B.P. Da Costa, R.A.P. Oliveira, J. Libardi, P.M. Faia, H.P. De Oliveira, TiO_2/ZnO hierarchical heteronanostructures: synthesis, characterization and application as photocatalysts, J. Environ. Chem. Eng. 4 (2016) 2820–2829, https://doi.org/10.1016/j.jece.2016.05.021.

[26] B. Pant, H.R. Pant, N.A.M. Barakat, M. Park, K. Jeon, Y. Choi, H.Y. Kim, Carbon nanofibers decorated with binary semiconductor (TiO_2/ZnO) nanocomposites for the effective removal of organic pollutants and the enhancement of antibacterial activities, Ceram. Int. 39 (2013) 7029–7035, https://doi.org/10.1016/j.ceramint.2013.02.041.

[27] Y.C. Huang, S.Y. Chang, C.F. Lin, W.J. Tseng, Synthesis of ZnO nanorod grafted TiO_2 nanotube 3-D arrayed heterostructure as supporting platform for nanoparticle deposition, J. Mater. Chem. 21 (2011) 14056–14061, https://doi.org/10.1039/c1jm11659b.

[28] C. Mondal, J. Pal, M. Ganguly, A.K. Sinha, J. Jana, T. Pal, A one pot synthesis of Au-ZnO nanocomposites for plasmon-enhanced sunlight driven photocatalytic activity, New J. Chem. 38 (2014) 2999–3005, https://doi.org/10.1039/c4nj00227j.

[29] A. Ghosh, P. Guha, A.K. Samantara, B.K. Jena, R. Bar, S. Ray, P.V. Satyam, Simple growth of faceted Au-ZnO hetero-nanostructures on silicon substrates (nanowires and triangular nanoflakes): a shape and defect driven enhanced photocatalytic performance under visible light, ACS Appl. Mater. Interfaces 7 (2015) 9486–9496, https://doi.org/10.1021/acsami.5b00634.

[30] C. Luo, D. Li, W. Wu, Y. Zhang, C. Pan, Preparation of porous micro-nano-structure NiO/ZnO heterojunction and its photocatalytic property, RSC Adv. 4 (2014) 3090–3095, https://doi.org/10.1039/c3ra44670k.

[31] D. Li, H. Haneda, Photocatalysis of sprayed nitrogen-containing Fe_2O_3-ZnO and WO_3-ZnO composite powders in gas-phase acetaldehyde decomposition, J. Photochem. Photobiol. A Chem. 160 (2003) 203–212, https://doi.org/10.1016/S1010-6030(03)00212-0.

[32] D. Li, H. Haneda, N. Ohashi, S. Hishita, Y. Yoshikawa, Synthesis of nanosized nitrogen-containing MOx-ZnO (M = W, V, Fe) composite powders by spray pyrolysis and their visible-light-driven photocatalysis in gas-phase acetaldehyde decomposition, Catal. Today (2004) 895–901, https://doi.org/10.1016/j.cattod.2004.06.099.

[33] N. Wei, H. Cui, X. Wang, X. Xie, M. Wang, L. Zhang, J. Tian, Hierarchical assembly of In_2O_3 nanoparticles on ZnO hollow nanotubes using carbon fibers as templates: enhanced photocatalytic and gas-sensing properties, J. Colloid Interface Sci. 498 (2017) 263–270, https://doi.org/10.1016/j.jcis.2017.03.072.

[34] K.S. Ranjith, R.B. Castillo, M. Sillanpaa, R.T. Rajendra Kumar, Effective shell wall thickness of vertically aligned ZnO-ZnS core-shell nanorod arrays on visible photocatalytic and photo sensing properties, Appl. Catal. B Environ. 237 (2018) 128–139, https://doi.org/10.1016/j.apcatb.2018.03.099.

[35] Z. Wang, S.W. Cao, S.C.J. Loo, C. Xue, Nanoparticle heterojunctions in ZnS-ZnO hybrid nanowires for visible-light-driven photocatalytic hydrogen generation, CrystEngCommun 15 (2013) 5688–5693, https://doi.org/10.1039/c3ce40523k.

[36] S. Khanchandani, P.K. Srivastava, S. Kumar, S. Ghosh, A.K. Ganguli, Band gap engineering of ZnO using core/shell morphology with environmentally benign Ag_2S sensitizer for efficient light harvesting and enhanced visible-light photocatalysis, Inorg. Chem. 53 (2014) 8902–8912, https://doi.org/10.1021/ic500518a.

[37] M.T. Uddin, Y. Nicolas, C. Olivier, L. Servant, T. Toupance, S. Li, A. Klein, W. Jaegermann, Improved photocatalytic activity in RuO_2-ZnO nanoparticulate heterostructures due to inhomogeneous space charge effects, Phys. Chem. Chem. Phys. 17 (2015) 5090–5102, https://doi.org/10.1039/c4cp04780j.

[38] M. Baek, E.J. Kim, S.W. Hong, W. Kim, K. Yong, Environmentally benign synthesis of $CuInS_2$/ZnO heteronanorods: visible light activated photocatalysis of organic pollutant/bacteria and study of its mechanism, Photochem. Photobiol. Sci. 16 (2017) 1792–1800, https://doi.org/10.1039/c7 pp00248c.

[39] S. Chabri, A. Dhara, B. Show, D. Adak, A. Sinha, N. Mukherjee, Mesoporous CuO-ZnO p-n heterojunction based nanocomposites with high specific surface area for enhanced photocatalysis and electrochemical sensing, Catal. Sci. Technol. 6 (2016) 3238–3252, https://doi.org/10.1039/c5cy01573a.

[40] A. Dhara, B. Show, A. Baral, S. Chabri, A. Sinha, N.R. Bandyopadhyay, N. Mukherjee, Core-shell CuO-ZnO p-n heterojunction with high specific surface area for enhanced photoelectrochemical (PEC) energy conversion, Sol. Energy 136 (2016) 327–332, https://doi.org/10.1016/j.solener.2016.07.022.

[41] M.M. Rahman, G. Gruner, M.S. Al-Ghamdi, M.A. Daous, S.B. Khan, A.M. Asiri, Chemo-sensors development based on low-dimensional codoped Mn_2O_3-ZnO nanoparticles using flat-silver electrodes, Chem. Cent. J. 7 (2013), https://doi.org/10.1186/1752-153X-7-60.

[42] W. Liu, M. Wang, C. Xu, S. Chen, X. Fu, Ag_3PO_4/ZnO: an efficient visible-light-sensitized composite with its application in photocatalytic degradation of Rhodamine B, Mater. Res. Bull. 48 (2013) 106–113, https://doi.org/10.1016/j.materresbull.2012.10.015.

[43] R. Saravanan, F. Gracia, M.M. Khan, V. Poornima, V.K. Gupta, V. Narayanan, A. Stephen, ZnO/CdO nanocomposites for textile effluent degradation and electrochemical detection, J. Mol. Liq. 209 (2015) 374–380, https://doi.org/10.1016/j.molliq.2015.05.040.

[44] S.M. Lam, J.C. Sin, I. Satoshi, A.Z. Abdullah, A.R. Mohamed, Enhanced sunlight photocatalytic performance over Nb_2O_5/ZnO nanorod composites and the mechanism study, Appl. Catal. A Gen. 471 (2014) 126–135, https://doi.org/10.1016/j.apcata.2013.12.001.

[45] T. Linda, S. Muthupoongodi, X. Sahaya Shajan, S. Balakumar, Photocatalytic degradation of congo red and crystal violet dyes on cellulose/ PVC/ZnO composites under UV light irradiation, Mater. Today Proc. (2016) 2035–2041, https://doi.org/10.1016/j.matpr.2016.04.106.

[46] H. Zhang, N. Patel, S. Ding, J. Xiong, P. Wu, Theranostics for hepatocellular carcinoma with Fe_3O_4@ZnO nanocomposites, Biomater. Sci. 4 (2016) 288–298, https://doi.org/10.1039/c5bm00361j.

[47] Y. Wang, Y. Wang, R. Xu, Photochemical deposition of Pt on CdS for H_2 evolution from water: markedly enhanced activity by controlling Pt reduction environment, J. Phys. Chem. C 117 (2013) 783–790, https://doi.org/10.1021/jp309603c.

[48] S. Min, Y. Lei, H. Sun, J. Hou, F. Wang, E. Cui, S. She, Z. Jin, J. Xu, X. Ma, Amorphous WSx as an efficient cocatalyst grown on CdS nanoparticles via photochemical deposition for enhanced visible-light-driven hydrogen evolution, Mol. Catal. 440 (2017) 190–198, https://doi.org/10.1016/j.mcat.2017.07.023.

[49] Y. Wu, T. Tamaki, T. Volotinen, L. Belova, K.V. Rao, Enhanced photoresponse of inkjet-printed ZnO thin films capped with CdS nanoparticles, J. Phys. Chem. Lett. 1 (2010) 89–92, https://doi.org/10.1021/jz900008y.

[50] X.F. Gao, W.T. Sun, Z.D. Hu, G. Ai, Y.L. Zhang, S. Feng, F. Li, L.M. Peng, An efficient method to form heterojunction CdS/TiO_2 photoelectrodes using highly ordered TiO_2 nanotube array films, J. Phys. Chem. C 113 (2009) 20481–20485, https://doi.org/10.1021/jp904320d.

[51] Y. Zhu, Y. Wang, Z. Chen, L. Qin, L. Yang, L. Zhu, P. Tang, T. Gao, Y. Huang, Z. Sha, G. Tang, Visible light induced photocatalysis on CdS quantum dots decorated TiO_2 nanotube arrays, Appl. Catal. A Gen. 498 (2015) 159–166, https://doi.org/10.1016/j.apcata.2015.03.035.

[52] M. Kokotov, G. Hodes, Influence of selective nucleation on the one step chemical bath deposition of CdS/ZnO and CdS/ZnS composite films, Chem. Mater. 22 (2010) 5483–5491, https://doi.org/10.1021/cm101248r.

[53] X. Cao, P. Chen, Y. Guo, Decoration of textured ZnO nanowires array with CdTe quantum dots: enhanced light-trapping effect and photogenerated charge separation, J. Phys. Chem. C 112 (2008) 20560–20566, https://doi.org/10.1021/jp806645c.

[54] P. Caballero, R. Reyes, J. Quirós, P. Macarrón, T. Lara, Calcinosis tumoral en la insuficiencia renal crónica, Rev. Clin. Esp. 179 (1986) 138–141, https://doi.org/10.1016/j.materresbull.2017.05.059.

[55] J.D. Patel, F. Mighri, A. Ajji, T.K. Chaudhuri, Development of CdS nanostructures by thermal decomposition of aminocaproic acid-mixed Cd-thiourea complex precursor: structural, optical and photocatalytic characterization, J. Nanosci. Nanotechnol. 15 (2015) 2733–2741, https://doi.org/10.1166/jnn.2015.9211.

[56] K. Rokesh, A. Nithya, K. Jeganathan, K. Jothivenkatachalam, A facile solid state synthesis of cone-like ZnO microstructure an efficient solar-light driven photocatalyst for rhodamine B degradation, Mater. Today Proc. (2016) 4163–4172, https://doi.org/10.1016/j.matpr.2016.11.091.

[57] G. Yang, Q. Zhang, W. Chang, W. Yan, Fabrication of Cd1-xZnxS/TiO_2 heterostructures with enhanced photocatalytic activity, J. Alloys Compd. 580 (2013) 29–36, https://doi.org/10.1016/j.jallcom.2013.05.083.

[58] M. Iqbal, A. Ali, N.A. Nahyoon, A. Majeed, R. Pothu, S. Phulpoto, K.H. Thebo, Photocatalytic degradation of organic pollutant with nanosized cadmium sulfide, Mater. Sci. Energy Technol. 2 (2019) 41–45, https://doi.org/10.1016/j.mset.2018.09.002.

[59] O.S. Bello, K.A. Adegoke, O.O. Akinyunni, Preparation and characterization of a novel adsorbent from Moringa oleifera leaf, Appl. Water Sci. 7 (2017) 1295–1305, https://doi.org/10.1007/s13201-015-0345-4.

[60] M. Fujii, K. Nagasuna, M. Fujishima, T. Akita, H. Tada, Photodeposition of CdS quantum dots on TiO_2: preparation, characterization, and reaction mechanism, J. Phys. Chem. C. 113 (2009) 16711–16716, https://doi.org/10.1021/jp9056626.

[61] B. Li, Y. Wang, Synthesis, microstructure, and photocatalysis of ZnO/CdS nano-heterostructure, J. Phys. Chem. Solids. 72 (2011) 1165–1169, https://doi.org/10.1016/j.jpcs.2011.07.010.

[62] H. Zhao, Y. Dong, P. Jiang, G. Wang, H. Miao, R. Wu, L. Kong, J. Zhang, C. Zhang, Light-assisted preparation of a ZnO/CdS nanocomposite for enhanced photocatalytic H_2 evolution: an insight into importance of in situ generated ZnS, ACS Sustain. Chem. Eng. 3 (2015) 969–977, https://doi.org/10.1021/acssuschemeng.5b00102.

[63] N. Soltani, E. Saion, M.Z. Hussein, M. Erfani, A. Abedini, G. Bahmanrokh, M. Navasery, P. Vaziri, Visible light-induced degradation of methylene blue in the presence of photocatalytic ZnS and CdS nanoparticles, Int. J. Mol. Sci. 13 (2012) 12242–12258, https://doi.org/10.3390/ijms131012242.

[64] L. Saikia, D. Bhuyan, M. Saikia, B. Malakar, D.K. Dutta, P. Sengupta, Photocatalytic performance of ZnO nanomaterials for self sensitized degradation of malachite green dye under solar light, Appl. Catal. A Gen. 490 (2015) 42–49, https://doi.org/10.1016/j.apcata.2014.10.053.

[65] A. Maavia, I. Aslam, M. Tanveer, M. Rizwan, M.W. Iqbal, M. Tahir, H. Hussain, R. Boddula, M. Yousuf, Facile synthesis of g-C_3N_4/$CdWO_4$ with excellent photocatalytic performance for the degradation of minocycline, Mater. Sci. Energy Technol. 2 (2019) 258–266.

[66] M. Iqbal, A.A. Thebo, A.H. Shah, A. Iqbal, K.H. Thebo, S. Phulpoto, M.A. Mohsin, Influence of Mn-doping on the photocatalytic and solar cell efficiency of CuO nanowires, Inorg. Chem. Commun. 76 (2017) 71–76, https://doi.org/10.1016/j.inoche.2016.11.023.

[67] K. Micheal, A. Ayeshamariam, R. Boddula, P. Arunachalam, M.S. AlSalhi, J. Theerthagiri, S. Prasad, J. Madhavan, A.M. Al-Mayouf, Assembled composite of hematite iron oxide on sponge-like BiOCl with enhanced photocatalytic activity, Mater. Sci. Energy Technol. 2 (2019) 104–111, https://doi.org/10.1016/j.mset.2018.11.004.

[68] S. Vadivel, B. Paul, D. Maruthamani, M. Kumaravel, T. Vijayaraghavan, S. Hariganesh, R. Pothu, Synthesis of yttrium doped BiOF/RGO composite for visible light: photocatalytic applications, Mater. Sci. Energy Technol. 2 (2019) 112–116, https://doi.org/10.1016/j.mset.2018.11.006.

[69] S. Yin, W. Fan, J. Di, T. Wu, J. Yan, M. He, J. Xia, H. Li, La^{3+}doped BiOBr microsphere with enhanced visible light photocatalytic activity, Colloids Surf. A Physicochem. Eng. Asp. (2017), https://doi.org/10.1016/j.colsurfa.2016.10.012.

[70] S. Sharifi-Asl, D.D. Macdonald, Electrochemical impedance spectroscopy, in: Dev. Electrochem. Sci. Inspired by Martin Fleischmann, 2014, https://doi.org/10.1002/9781118694404.ch19.

[71] E.P. Randviir, C.E. Banks, Electrochemical impedance spectroscopy: an overview of bioanalytical applications, Anal. Methods (2013), https://doi.org/10.1039/c3ay26476a.

[72] Y. Tak, S.J. Hong, J.S. Lee, K. Yong, Fabrication of ZnO/CdS core/shell nanowire arrays for efficient solar energy conversion, J. Mater. Chem. (2009), https://doi.org/10.1039/b904993b.

[73] A.I. Persson, M.W. Larsson, S. Stenström, B.J. Ohlsson, L. Samuelson, L.R. Wallenberg, Solid-phase diffusion mechanism for GaAs nanowire growth, Nat. Mater. (2004), https://doi.org/10.1038/nmat1220.

[74] D. Barpuzary, Z. Khan, N. Vinothkumar, M. De, M. Qureshi, Hierarchically grown urchinlike CdS@ZnO and CdS@Al_2O_3 heteroarrays for efficient visible-light-driven photocatalytic hydrogen generation, J. Phys. Chem. C (2012), https://doi.org/10.1021/jp207452c.

[75] S. Khanchandani, S. Kundu, A. Patra, A.K. Ganguli, C.S. Nanorods, S. Khanchandani, S. Kundu, A. Patra, A.K. Ganguli, Shell thickness dependent photocatalytic properties of ZnO / CdS, J. Phys. Chem. (2012), https://doi.org/10.1021/jp3083419.

[76] P. Sudhagar, S. Chandramohan, R.S. Kumar, R. Sathyamoorthy, C.H. Hong, Y.S. Kang, Fabrication and charge-transfer characteristics of CdS QDs sensitized vertically grown flower-like ZnO solar cells with CdSe cosensitizers, Phys. Status Solidi Appl. Mater. Sci. (2011), https://doi.org/10.1002/pssa.201026276.

[77] Q. Yuan, L. Chen, M. Xiong, J. He, S.L. Luo, C.T. Au, S.F. Yin, Cu_2O/$BiVO_4$ heterostructures: Synthesis and application in simultaneous photocatalytic oxidation of organic dyes and reduction of Cr(VI) under visible light, Chem. Eng. J. (2014), https://doi.org/10.1016/j.cej.2014.06.031.